

Robust Construction of Polycube Segmentations via Dual Loops

M. Snoep, B. Speckmann, and K. Verbeek

TU Eindhoven, The Netherlands

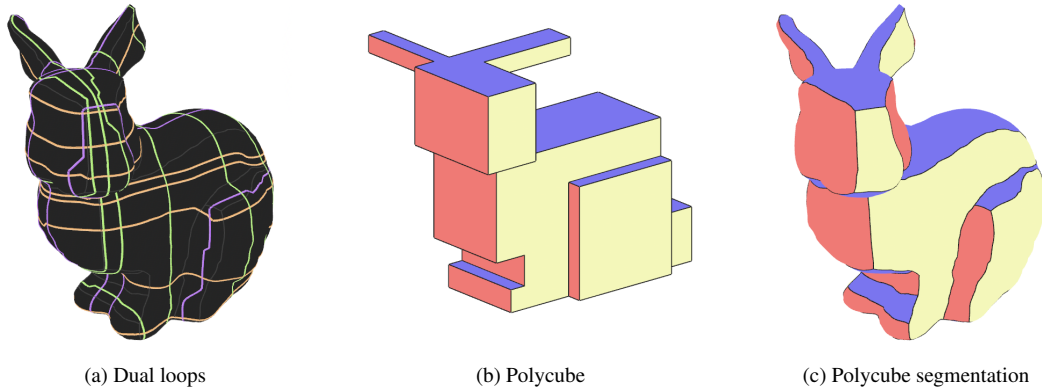


Figure 1: The dual approach for the construction of polycube segmentations.

Abstract

Polycube segmentations for 3D models effectively support a wide variety of applications such as seamless texture mapping, spline fitting, structured multi-block grid generation, and hexahedral mesh construction. However, the automated construction of valid polycube segmentations suffers from robustness issues: state-of-the-art methods are not guaranteed to find a valid solution. In this paper we present an iterative algorithm which is guaranteed to return a valid polycube segmentation for 3D models of any genus. Our algorithm is based on a dual representation of polycubes. Starting from an initial simple polycube of the correct genus, together with the corresponding dual loop structure and polycube segmentation, we iteratively refine the polycube, loop structure, and segmentation, while maintaining the correctness of the solution. Our algorithm is robust by construction: at any point during the iterative process the current segmentation is valid. Furthermore, the iterative nature of our algorithm facilitates a seamless trade-off between quality and complexity of the solution. Our algorithm can be implemented using comparatively simple algorithmic building blocks; our experimental evaluation establishes that the quality of our polycube segmentations is on par with, or exceeding, the state-of-the-art.

1. Introduction

Polycubes are orthogonal polyhedra with axis-aligned quadrilateral faces. The simple structure of polycubes enables efficient solutions to various challenging geometric problems. Bijective mappings from general shapes to polycubes, known as *polycube maps*, enable the transfer of solutions computed on polycubes to those general shapes. Polycube maps are used to solve problems such as texture mapping [THCM04], spline fitting [WHL*07], multi-block grid generation [BBG*09], and hexahedral meshing [PCS*22].

Formally, a polycube map f is a continuous map from a polycube Q of genus g to a closed 2-dimensional surface \mathcal{M} of the same genus. The edges of Q map to a segmentation of \mathcal{M} into *patches*

that correspond to the faces of Q , known as a *polycube segmentation* (see Figure 1). Each patch has a *label* $\pm X / \pm Y / \pm Z$: the direction of the normal vector of its corresponding polycube face.

Since their introduction in 2004 [THCM04], numerous methods have been proposed for constructing polycube maps. The quality of a polycube map is determined by two competing factors: the complexity of the polycube and the distortion of the mapping. Methods that construct polycube maps must find a balance between these conflicting factors. The state-of-the-art achieves a good trade-off between low distortion and low complexity [GSZ11, LVS*13, DPM*22].

A common approach for constructing polycube maps is to directly construct a polycube segmentation [DPM*22, FBL16, GSZ11, HZ16, HZL17, LVS*13, ZLL*17]. We call this the *primal* approach. Developing a polycube segmentation into a full (surface or volume) polycube map can be done via various established methods [GSZ11, PRR*22].

The proposed methods for constructing polycube segmentations [SR15, ZLW*19, PRR*22, MPBL23] suffer from various robustness issues. The methods incorrectly identify invalid segmentations as valid, and vice-versa, since they can not guarantee that the constructed polycube segmentations are valid. The existing *characterizations* of polycubes [EM10, HLW*24, ZLW*19], used for checking whether a segmentation corresponds to a valid polycube, are neither necessary nor sufficient [MPBL23, Sok16, SSV25]. As a result, current primal methods unnecessarily restrict their solution space or generate invalid solutions.

In this paper we describe an iterative robust algorithm to construct polycube segmentations. Our algorithm is based on a recent characterization of polycubes via its dual loop structure [SSV25]. This characterization is complete, but characterizes a specific subset of polycubes: those with strictly quadrilateral faces. This does not necessarily restrict the space of shapes we can form, but requires us to construct such polycube segmentations in order to use their characterization. The characterization is not directly applicable to the previously mentioned approaches, as they construct polycube segmentations with arbitrarily complex patches. Note that we can turn quad-only polycube segmentations into the arbitrarily-complex polycube segmentations by simply "hiding" the so-called *flat edges*, edges between two patches with the same label.

We start with a simple loop structure that corresponds to a polycube that has the same genus as the input surface \mathcal{M} . Then we iteratively *add* or *remove* loops to refine or simplify the loop structure in a way that preserves validity. The iterative nature of our algorithm allows us to explicitly control the trade-off between the complexity of the polycube and the distortion of the mapping. We review related work in Section 2 and give the necessary mathematical background, including the dual representation of polycubes, in Section 3. In Section 4 we describe our algorithm in detail. In Section 5 we evaluate our algorithm experimentally. Finally, we conclude with avenues for future work in Section 6.

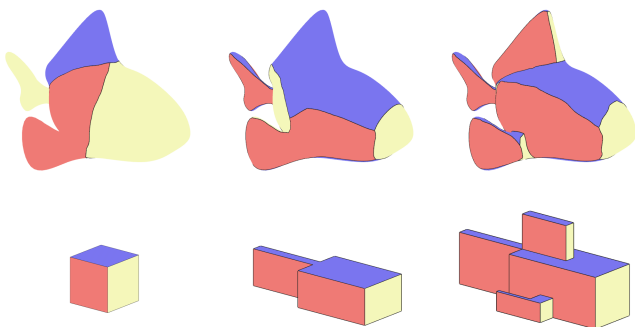


Figure 2: Our iterative process, akin to the development of an egg to a guppy to an adult fish.

2. Related Work

In 2004 [THCM04] introduced polycube maps as an extension of cube maps. Since polycube maps proved to be an effective tool to solve challenging problems such as hexahedral meshing, many methods have been proposed to automate their construction. The first methods by [THCM04] and [WHL*08] constructed polycube maps from manually constructed polycubes. The first fully automatic construction methods had significant drawbacks, as they produced polycubes that were either very coarse [LJFW08] or very detailed [HWFQ09].

The most prominent methods for polycube map construction are based on the deformation approach by [GSZ11] which was later improved or extended by many [LVS*13, HJS*14, YZWL14, YFL19, FBL16, DPM*22, ZLW*19, FXBH16, GLYL20, MCBC22, CLS16]. The deformation-based approaches find an initial polycube segmentation in various ways, none of which guarantees that the segmentation corresponds to a valid polycube. Then, the input shape is gradually deformed until the surface faces are oriented toward their assigned target label. The initial polycube labeling may be adjusted during the deformation process. Many deformation methods use the characterization of orthogonal polyhedra by [EM10] to increase their robustness. However, this characterization is neither sufficient nor necessary for valid polycubes [SR15, MCBC22, PCS*22, MPBL23].

An alternative set of methods is based on voxelization [WYZ*11, YFL19, YZWL14]. In general, a polycube map can be obtained by projecting a voxelized version of \mathcal{M} back onto \mathcal{M} . Although voxelizing \mathcal{M} yields a valid polycube, the projection cannot be done robustly and may fail to preserve the topology of \mathcal{M} . Furthermore, voxelization results in overly detailed polycubes, which is not desirable for most downstream applications.

Finally, since polycube maps are popular for solving the hexahedral meshing problem, some methods focus on optimizing specifically for hexahedral meshing. These methods obtain more manageable input surfaces that result in higher quality hexahedral meshes by introducing cuts or deforming the input surface [FXBH16, GLYL20, MCBC22]. While this works for hexahedral meshing of the interior volume of shapes, the methods are not suitable for other downstream applications (such as multi-block grid generation) where preservation of topology and low distortion with the original input model are crucial.

A different line of work by Baumeister and Kobbelt [BK23] and Snoep et al. [SSV25] (building on insights from Biedl and Genc [BG04]), takes a *dual* approach. Rather than directly constructing polycube segmentations, they first establish a valid dual structure on \mathcal{M} that is then *primalized* into a guaranteed valid polycube segmentation. This idea mirrors the dual approach in quad meshing [CBK12]. While experiments suggest this method can work, the practical aspects of implementing a complete pipeline, along with its limitations and how it compares to existing solutions, have yet to be fully explored.

3. Polycubes via Dual Loops

The algorithm in this paper is based on the characterization of polycubes by Snoep, Speckmann, and Verbeek [SSV25]. In this section we review the necessary definitions and results from their work.

A *quadrilateral mesh* (*quad mesh*) consists of vertices, edges, and quadrilateral faces. Each vertex is adjacent to at least one edge. Each edge is adjacent to one or two faces. Each face consists of four vertices and four edges. A quad mesh is *closed* if each edge is adjacent to exactly two faces. A quad mesh is *orientable* if a consistent circular ordering of vertices can be assigned to each face, such that edge-adjacent faces have opposite vertex orders along their common edge. A quad mesh is *connected* if every vertex can be reached from any other vertex by traversing edges. We can now define a polycube (see Definition 1 and Figure 3).

Definition 1 A *polycube* Q is a closed, connected, orientable quad mesh with vertices $V(Q)$ such that:

1. Each vertex $v \in V(Q)$ has a position $p(v)$ in \mathbb{Z}^3 ,
2. Each vertex has degree at least 3,
3. Positions of adjacent vertices differ in exactly one coordinate,
4. Edges incident to the same vertex cannot overlap.

Each polycube defines three partial orders on its vertices, corresponding to the three principal axes (X , Y , and Z). The partial order for the X -axis is defined as follows: for two vertices v and w , we say that $v \leq_X w$ if the x -coordinate of v is less than or equal to the x -coordinate of w , and there is an edge between v and w . The partial orders for the Y -axis and Z -axis are defined similarly.

Definition 2 Two polycubes Q_1 and Q_2 are *order-equivalent* if there exists an isomorphism $f: V(Q_1) \rightarrow V(Q_2)$ between the quad meshes of Q_1 and Q_2 such that, for all $v, w \in V(Q_1)$ and $\Delta \in \{X, Y, Z\}$, we have that $v \leq_\Delta w$ if and only if $f(v) \leq_\Delta f(w)$.

3.1. Dual structure

Polycubes exhibit a dual loop structure, where each loop represents a strip of quadrilateral faces whose center points share a single coordinate [BG04]; see Figure 4. This structure forms a system of intersecting loops. The places where two loops intersect are called *loop intersections*. The parts of a loop bounded by two intersection points (but containing no intersection points) are called *loop segments*. The areas bounded by loop segments are called *loop regions*. Note that each loop region of a polycube corresponds to exactly one corner of the polycube.

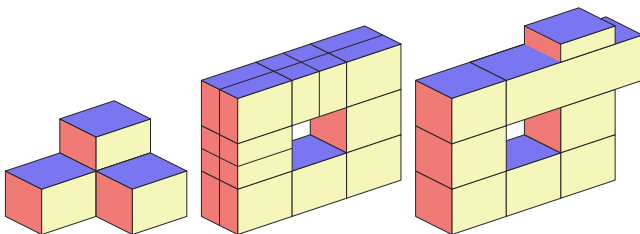


Figure 3: The variety of polycubes that satisfy Definition 1. Note that polycubes are in principle allowed to globally self-intersect.

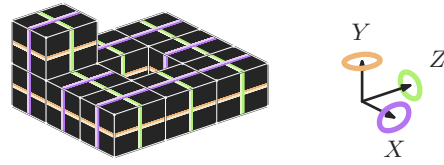


Figure 4: A polycube and its oriented X -, Y -, and Z -loops.

If you consider the normals of the quadrilateral faces of a single loop, they always correspond to exactly two axes ($\{X, Y, Z\}$). As such, the loops can be labeled as either an X -, Y -, or Z -loop as follows: an X -loop traverses faces with normals aligned to Y - and Z -axes. The Y - and Z -loops are similarly defined.

Furthermore, each loop is oriented with a defined *positive* and *negative* side. Crossing a loop on the polycube from its negative to positive side corresponds to an increase in coordinates on the polycube vertices. Crossing in the opposite direction results in a decrease. In our figures, we use the colors purple, lighter purple, orange, lighter orange, green, and lighter green for $+X$, $-X$, $+Y$, $-Y$, $+Z$, and $-Z$, respectively. See Figure 4.

We can use the full set of X -loops of an oriented loop structure to partition the underlying space (surface or polycube) into regions. We refer to these regions as *X -zones*. We can use these zones to capture the global structure of the polycube (with regard to the X -axis) in a directed graph. Specifically, the *X -graph* has a vertex for each X -zone, and a directed edge (u, v) for every X -loop with u and v corresponding to the X -zones on the negative and positive side of the loop, respectively. We can define the Y -zones, Z -zones, Y -graph and Z -graph similarly.

3.2. Characterization

Consider a loop structure embedded on some arbitrary surface (not necessarily a polycube). In the remainder of this paper we implicitly assume that each loop in a loop structure is both oriented (defining negative and positive sides) and labeled with either X , Y , or Z , unless stated otherwise. There exists a complete set of rules that characterize which of these loop structures correspond to *polycube loop structures*; that is, the loop structures that are dual to a polycube.

Definition 3 A loop structure is a *polycube loop structure* if:

1. No three loops intersect at a single point.
2. Each loop region is bounded by at least three loop segments.
3. Within each loop region boundary, no two loop segments have the same axis label *and* side label.
4. Each loop region has the topology of a disk.
5. The X -, Y -, and Z -graphs are acyclic.

The following result was shown by Snoep *et al.*

Theorem 1 ([SSV25]) For every polycube Q there exists a polycube loop structure \mathcal{L} that forms the dual of Q . Furthermore, given a polycube loop structure \mathcal{L} , there exists exactly one polycube Q (up to order-equivalence) that corresponds to \mathcal{L} .

4. Algorithm

In this section we present our algorithm for computing polycube segmentations of triangulated 3D models. We first give a general overview of the algorithm, before we dive deeper into the most important parts of the algorithm: adding loops to a polycube loop structure, computing the polycube segmentation from a polycube loop structure, and optimizing the polycube loop structure.

The input to our algorithm is a 3D model represented as a triangulated surface mesh $\mathcal{M} = (V, T)$, where V is the set of vertices and T is the set of triangular faces, each defined by a triplet (v_i, v_j, v_k) of vertices. The edges of \mathcal{M} are implicitly defined by the faces. We assume that \mathcal{M} is a well-formed, orientable, manifold surface of arbitrary genus that bounds a single volume. Additionally, \mathcal{M} is embedded in \mathbb{R}^3 , meaning that every vertex $v \in V$ has an associated position $p(v) = (x(v), y(v), z(v)) \in \mathbb{R}^3$, and each triangle $t \in T$ has a corresponding normal vector $n(t)$.

Our goal is to compute a *polycube segmentation* $S(\mathcal{M}) = (C, \mathcal{P})$ of \mathcal{M} . Here, C is a set of points on \mathcal{M} representing *corners*, and \mathcal{P} is a collection of *paths* embedded on \mathcal{M} connecting these corners. These paths do not intersect each other and partition \mathcal{M} into *patches*, forming quadrilateral subsurfaces. The corners and paths do not necessarily consist of the elements (vertices and edges) of \mathcal{M} , but must lie on the surface defined by \mathcal{M} . In general, a corner can be positioned anywhere on a face of \mathcal{M} and a path can traverse the interior of faces of \mathcal{M} . Each patch has an assigned *label* corresponding to one of the six (signed) principal axes: $\pm X / \pm Y / \pm Z$. A segmentation S qualifies as a polycube segmentation if there exists a polycube Q whose vertices, edges, and faces correspond one-to-one with the corners, paths, and patches of S . Furthermore, the label of each patch must correspond to the normal vector of its associated polycube face.

Our algorithm does not compute a polycube segmentation directly, but instead focuses on computing a valid (polycube) loop structure \mathcal{L} . The loops of \mathcal{L} are directly embedded on the surface mesh \mathcal{M} . By ensuring that \mathcal{L} satisfies the properties of Definition 3, we can guarantee that we can compute a polycube segmentation from \mathcal{L} at any step of the algorithm. Our algorithm now proceeds as follows. First, we initialize a loop structure of minimum complexity on \mathcal{M} . For a model of genus zero, this is simply a loop structure consisting of three loops (one for each axis label), which corresponds to a single cube as polycube. For models of higher genus, this initialization is more involved (see Section 4.3 for more details). Next, we alter the loop structure by adding or removing loops. In Section 4.1 we explain in detail how to find good loops that improve the quality of the polycube segmentation, and at the same time preserve the characterization of a polycube loop structure stated in Definition 3. Once we have obtained a good loop structure, we compute a corresponding polycube segmentation by placing a corner in every loop region, and connecting the corners of adjacent loop regions via non-intersecting paths on \mathcal{M} . We refer to this process as *primalization* and discuss this step in more detail in Section 4.2. To obtain the best loop structure \mathcal{L} , we actually maintain a collection of loop structures, and we utilize a type of evolutionary algorithm to optimize the quality of the corresponding polycube segmentations (see Section 4.3 for details).

Observe that our algorithm does not actually compute the corresponding polycube of the polycube segmentation. However, our approach makes it relatively straightforward to compute the corresponding unique polycube (up to order-equivalence), and hence we often include the corresponding polycubes in our figures for clarity. Since this is not the main purpose of our algorithm, we will not describe how to compute these polycubes, and we will not try to optimize their exact geometric representation.

To find the best loop structure via our evolutionary algorithm, we need to define the *quality* of a polycube segmentation. There is no single standard for measuring the quality of a polycube segmentation, as different applications have different requirements. Polycube maps are commonly used in hexahedral meshing, spline fitting, and structured multi-block grid generation, each prioritizing different aspects such as minimal distortion or fewer patches in the segmentation. In general, existing approaches seek to balance *complexity*, often tied to the number of vertices in the corresponding polycube, and *distortion*, which captures how well the polycube map transforms the original surface into the polycube. In this paper we specifically choose to optimize the following two criteria.

Alignment: This aspect captures how well the segmentation aligns with the original mesh geometry. Specifically, we use the angular deviation between the normal of each triangle and its assigned label.

Complexity: This aspect captures the complexity of the polycube segmentation. Since our algorithm focuses on computing a loop structure, we measure the complexity via the number of loops in the loop structure. Although there is no direct relation between the number of loops and the complexity of the resulting polycube segmentation, the number of loops acts as a good proxy.

In Section 4.3 we discuss which exact metrics we use and how we handle the resulting multi-objective optimization problem. Note that the alignment cannot directly be computed on a loop structure, but it depends on a polycube segmentation. Therefore, whenever our algorithm evaluates the quality of a loop structure, it has to compute a corresponding polycube segmentation through the primalization step.

4.1. Adding loops

In this section we describe how we can compute a suitable loop ℓ to add to an existing loop structure \mathcal{L} . Without loss of generality we can assume that ℓ has axis label X . To add a suitable loop, we need to consider two main aspects: (1) the alignment of the loop, to ensure that the resulting patches in the polycube segmentation will also align well; and (2) the validity of the loop, to ensure that the resulting loop structure $\mathcal{L} \cup \{\ell\}$ is also a polycube loop structure. Before we discuss these aspects in detail, we first consider the representation of loops in \mathcal{L} embedded on \mathcal{M} .

Representation. Technically speaking, it is possible to represent any possible loop ℓ on \mathcal{M} as a function $f: S^1 \rightarrow \mathcal{M}$. However, the continuous search space makes it computationally difficult and expensive to find suitable loops. Instead, we would like to use a discretization of \mathcal{M} to restrict the set of possible loops. A natural choice would be to restrict loops to the vertices and edges of \mathcal{M} .

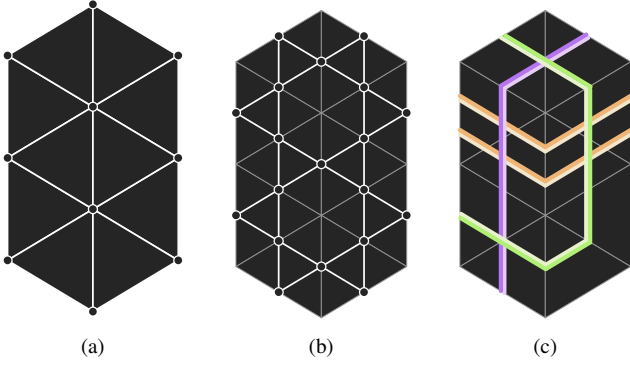


Figure 5: A triangular mesh \mathcal{M} (a) and its edge graph G (b). We compute loops on the edge graph, which results in loops crossing the edges of \mathcal{M} transversally (c).

However, using this approach, two different loops cannot use the same edge of \mathcal{M} . If we would allow two loops to share the same edge, then this could result in ambiguous overlaps between loops and degenerate loop regions. As a result, we may be unable to find any valid loop due to this restriction, making it overly restrictive.

Instead, we want to use a representation of loops that allows us to always add another loop to the loop structure. To that end, we represent a loop ℓ by the sequence of edges of \mathcal{M} that are crossed transversally by ℓ . Now, if two different loops cross the same edge e of \mathcal{M} , we can easily separate them along e when needed (assuming that we know the order of the loops along e). Specifically, a loop is then represented by a sequence $[e_0, \dots, e_n]$ of edges of \mathcal{M} , where $e_0 = e_n$ and where e_i and e_{i+1} share a triangle on \mathcal{M} for $0 \leq i < n$. Additionally, for each edge e of \mathcal{M} , we keep track of the set of loops that cross e and in which order. Using this combinatorial representation of the loops, we can easily realize the loops geometrically without introducing overlaps or degenerate loop regions, and it is always possible to add another loop (see Figure 5).

To make it easy to work with this representation of loops, we construct the *edge graph* $G = (V, E)$ of \mathcal{M} . In the edge graph G , every node represents an edge of \mathcal{M} , and there is an edge between two nodes if the corresponding edges share a triangle in \mathcal{M} (see Figure 5). We also assign a position to the nodes in G : if $e = (u, v)$ is an edge of \mathcal{M} (and hence a node in G), then we define $p(e) = (p(u) + p(v))/2$. Now, every loop ℓ using the representation chosen above simply corresponds to a path in G .

Alignment. A good alignment of the final polycube segmentation can be achieved by creating a polycube map with small distortion. If we consider a loop ℓ with axis label X , then this corresponds to an X -loop on a polycube \mathcal{Q} . Recall that all points on an X -loop have the same x -coordinate. Equivalently, all points on an X -loop lie in a single plane perpendicular to the X -axis. Thus, to achieve good alignment, the loop ℓ should have similar properties.

Now consider a point p on loop ℓ . Let $d(p)$ be the tangent vector at p in the direction of traversal of ℓ , and let $n(p)$ be the normal vector at p with respect to \mathcal{M} . If ℓ were an X -loop on a polycube, then both $d(p)$ and $n(p)$ would be perpendicular to the X -axis. Equiva-

lently, the cross product $d(p) \times n(p)$ would align with the X -axis. Therefore, for a good loop ℓ with axis label X , we would like the angle between $d(p) \times n(p)$ and the X -axis to be small for all points p on ℓ .

We now formulate the problem of finding a good loop ℓ on \mathcal{M} as a shortest path problem on the edge graph G . To that end, we assign a weight function w_X to the edges of G . For an edge (e, e') of G , let $d(e, e') = p(e') - p(e)$ and let $n(e, e')$ be the normal vector of the shared triangle of e and e' on \mathcal{M} . We define w_X as follows.

$$w_X(e, e') = \text{angle}(d(e, e') \times n(e, e'), \vec{X})^\alpha$$

Here, the function $\text{angle}(\cdot, \cdot)$ measures the angle between two vectors in radians, and \vec{X} is the unit vector in positive X direction. Furthermore, $\alpha > 1$ is the *strictness factor*, on which we elaborate further below. Observe that this weight function is not symmetric, that is, $w_X(e, e') \neq w_X(e', e)$. This is necessary to enforce the loop to follow a specific orientation (clockwise), and to traverse fully around the surface mesh \mathcal{M} . We can define weight functions w_Y and w_Z for the other axis labels analogously.

We can now compute a loop ℓ by first choosing a starting node e in G , and then computing the shortest non-empty path from e to itself in G using the weight function w_X . To enforce the loop to traverse fully around \mathcal{M} , we need to make sure that misaligned edges are sufficiently penalized, for otherwise the loop would simply return directly. This can be achieved by setting the strictness factor sufficiently high.

Validity. A loop ℓ computed in G may not be valid, that is, adding ℓ to \mathcal{L} may not result in a valid polycube loop structure. The validity of a loop depends on its *topological structure*. The topological structure of a loop ℓ is defined by the sequence of loop regions of \mathcal{L} visited by ℓ . In [SSV25] it is shown how to efficiently determine if the topological structure of a loop is valid, and how to enumerate all valid (topological structures of) loops that can be added to \mathcal{L} .

We now compute a valid loop ℓ in G as follows. First, we use the results of [SSV25] to choose a topological structure that corresponds to a valid loop. This topological structure then determines the sequence of loop regions in \mathcal{L} that must be visited by ℓ . We observe that each loop region can be visited at most once in this sequence. Thus, we can enforce this topological structure in G as follows: for every two consecutive loop regions R_i and R_{i+1} in the sequence, we remove all (directed) edges from G that go from R_i to another loop region that is not R_{i+1} . Now we can use this restricted version of G to compute the most aligned loop ℓ that has the chosen topological structure.

To find the best loop possible to add to \mathcal{L} , we should try all possible topological structures that correspond to a valid loop. However, as already shown in [SSV25], there may be an exponential number of valid topological structures. We therefore restrict our search to a limited set of topological structures. For each loop region R in \mathcal{L} , we consider only the topological structure that visits the fewest loop regions. This approach limits the number of possible valid loops (of some specific axis label) to the number of loop regions in \mathcal{L} .

4.2. Primalization

In this section we describe how we perform the primalization step, that is, how we compute the polycube segmentation $S(\mathcal{M}) = (C, \mathcal{P})$ from the polycube loop structure \mathcal{L} . The primalization step consists of two main aspects: (1) placing a corner in each loop region R of \mathcal{L} , and (2) computing (non-intersecting) paths between corners of adjacent loop regions.

Corner placement. Before we can place corners in loop regions, we first ensure that every loop region contains at least one vertex. To that end, we refine the mesh \mathcal{M} into a mesh \mathcal{M}' by adding the loops in \mathcal{L} to \mathcal{M} (properly separated) and by further subdividing loop regions without internal vertices. To find the best vertex $v \in \mathcal{M}'$ on which to place a corner, we use two main criteria: (1) The local neighborhood of v in \mathcal{M}' should be as similar as possible to the local neighborhood of the corresponding corner in the polycube \mathcal{Q} (see Figure 6); (2) Corners that belong to the same zone should be placed on vertices with similar coordinates. Specifically, if two corners belong to the same X -zone in the corresponding polycube \mathcal{Q} , then they should be placed on vertices in \mathcal{M}' with a similar x -coordinate (see Figure 7).

We satisfy these two criteria using a two-step process. First, for every loop region R , we compute a candidate set $\mathcal{C}(R)$ of vertices based on the first criterion. Next, we choose the best vertices from each candidate set that optimize the second criterion.

For the first step, consider a loop region R and let c be the corresponding corner of the polycube \mathcal{Q} . The corner c is incident to a number of faces in \mathcal{Q} that are perpendicular to one of the (signed) principal axes: $-X, +X, -Y, +Y, -Z, +Z$. Let $L(c)$ be the set of face types of all faces incident to c in \mathcal{Q} . Now consider a triangle t of \mathcal{M}' in R . We can also assign a label among $\{-X, +X, -Y, +Y, -Z, +Z\}$ to t based on which principal direction is closest to the normal $n(t)$. Then, for each vertex v , we can similarly define $L(v)$ as the set of all labels of triangles incident to v on \mathcal{M}' . We now define the similarity $s_c(v)$ of v with respect to c :

$$s_c(v) = |L(v) \cap L(c)| - |L(v) \setminus L(c)|$$

The candidate set $\mathcal{C}(R)$ simply consists of all vertices v in R that achieve the highest similarity score $s_c(v)$ over all vertices in R .

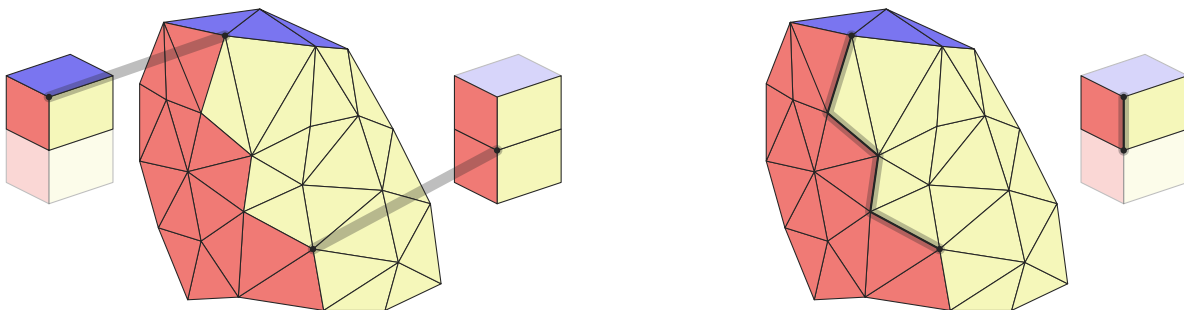


Figure 6: Polycube corners should align with vertices having similar face normals. Patch boundaries should follow mesh edges where adjacent face normals resemble those along the polycube edge.

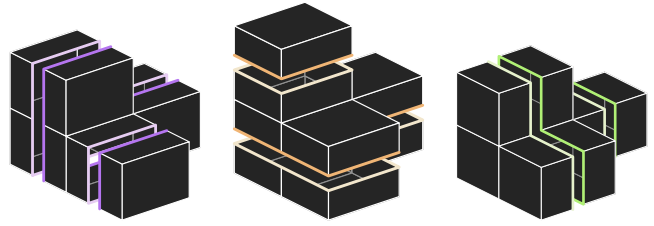


Figure 7: Polycube corners in the same zone share a coordinate.

For the second step, we need to consider the zones to which the loop regions belong. Let ζ_x be an X -zone and let R_1, \dots, R_k be the loop regions that belong to ζ_x . We first compute the smallest interval $I(\zeta_x) = [x^-, x^+]$ such that there exists a vertex $v \in \mathcal{C}(R_i)$ with $x(v) \in I$ for all $i \in [1, k]$. We can compute this interval efficiently by first sorting the candidate vertices of the respective loop regions on x -coordinate, and then maintaining a valid interval using two pointers, as we move the left endpoint of the interval over all possible x -coordinates in increasing order. Let $m(\zeta_x)$ be the midpoint of the interval $I(\zeta_x)$.

Now again consider a single loop region R . This loop region must be part of exactly one X -zone ζ_x , one Y -zone ζ_y , and one Z -zone ζ_z . To choose the vertex v on which to place the corner of R , we simply pick the vertex $v \in \mathcal{C}(R)$ that minimizes the Euclidean distance between $p(v)$ and $p^* = (m(\zeta_x), m(\zeta_y), m(\zeta_z))$.

Paths. The next step is to compute non-intersecting paths connecting the corners of adjacent loop regions. We compute these paths incrementally (one after the other), which is both efficient and results in high-quality paths. To give these paths enough freedom to route between corners, we allow them to route on both the edge graph of \mathcal{M}' and on the vertices and edges of \mathcal{M}' itself. Specifically, we construct a graph G^+ from \mathcal{M}' , where every node of G^+ corresponds to either a vertex or edge of \mathcal{M}' , and where two nodes of G^+ are connected by an edge if one of the following holds: (1) the two corresponding vertices are connected by an edge in \mathcal{M}' , (2) the two corresponding edges share a triangle in \mathcal{M}' , or (3) the corresponding vertex/edge pair shares a triangle in \mathcal{M}' .

We compute the paths (roughly) in order from shortest to longest, where we use the Euclidean distance between corners as a proxy for the length of the path between them. Consider computing the path P between the two corners at v and v' or R and R' , respectively. Similar to the corner placement, we have two main quality criteria: (1) the local neighborhood around P should be as similar as possible to the local neighborhood of the corresponding edge in polycube Q , and (2) the length of P should be as short as possible. The second criterion can easily be achieved by turning G^+ into a weighted graph, where the weight of an edge is determined by the Euclidean distance between its endpoints (note that every node in G^+ has a position in \mathbb{R}^3). To ensure that P crosses only the loop segment between R and R' , we exclude all edges from G^+ that cross another loop segment. Similarly, to avoid intersecting with already computed paths, we exclude the edges of other paths as well. We can then compute P via a shortest-path algorithm.

To also incorporate the first quality criterion, we adapt the weights of the edges of G^+ based on the orientation of the incident triangles on \mathcal{M}' . If we consider the edge of the polycube Q that corresponds to P , then the normals of the incident faces left and right from the edge are constant in Q and align with one of the principal axes (see Figure 6). Let these normals be n_l and n_r , respectively. Similarly, for a directed edge e of G^+ , we consider the triangles t_l and t_r to the left and right of e , respectively. Note that, if e is not an edge of \mathcal{M}' , then e lies on a single triangle t of \mathcal{M}' , and we define $t_l = t_r = t$. We define alignment penalties $a_l(e)$ and $a_r(e)$ for the left and right side of an edge e , respectively, where $a_l(e)$ is defined as:

$$a_l(e) = \begin{cases} 1 & \text{if } n_l \cdot n(t_l) \leq 1/\sqrt{3} \\ \text{angle}(n_l, n(t_l))^2 & \text{otherwise} \end{cases}$$

Note that the alignment penalty is 1 (no penalty) if the angle between n_l and $n(t_l)$ is smaller than $\arccos 1/\sqrt{3} \approx 0.955$ radians. This is the largest angle between a normal vector and its most similar principal direction. The penalty $a_r(e)$ is defined analogously. We now adapt the weight of e by multiplying its current weight (Euclidean distance) by $(a_l(e) + a_r(e))/2$.

We can now compute a path P between two adjacent corners by finding the shortest path in G^+ with the given weights. Afterwards, we add the edges of P to the underlying mesh \mathcal{M}' , and update \mathcal{M}' and G^+ accordingly. We repeat this process until all paths have been computed, after which we obtain a valid polycube segmentation. Note that it is straightforward to assign labels ($\pm X / \pm Y / \pm Z$) to the triangles/patches of \mathcal{M}' given the placement of the corners, the paths, and the loop structure.

4.3. Loop structure optimization

In this section we describe our evolutionary algorithm for finding a good polycube loop structure. We first describe how to initialize a valid polycube loop structure, then we establish the optimization function for polycube loop structure, and finally we discuss the details of our evolutionary algorithm.

Initialization. For models of genus zero, the initial polycube loop structure should correspond to a single cube as polycube. This means that the loop structure has exactly one X -loop, one Y -loop,

and one Z -loop. We can use the approach of Section 4.1 to add these 3 loops in arbitrary order. Note that the topological structures of these initial loops are fixed, although we can still choose in which loop regions we start the search.

For models of higher genus, initialization is significantly more challenging. There are multiple possible corresponding polycubes of minimum complexity, and it is also important to choose the right orientation of the holes in the model. We therefore initialize these loop structures by choosing the topological structures of the initial loops manually. We leave the automated initialization of loop structures for higher-genus models to future work.

Optimization function. As already discussed at the start of Section 4, we consider two optimization criteria: alignment and complexity. The complexity $f_c(\mathcal{L})$ of a loop structure \mathcal{L} is simply measured by the number of loops. To compute the alignment, we first need to primalize the loop structure \mathcal{L} . Then, for each triangle t in the resulting mesh \mathcal{M}' , we consider its normal $n(t)$ and the vector $l(t)$ that corresponds to the label given to t by the polycube segmentation. Let $f_a(t)$ be the alignment between $n(t)$ and $l(t)$ computed using the dot product:

$$f_a(t) = n(t) \cdot l(t)$$

Observe that the dot product measures the cosine of the angle between $n(t)$ and $l(t)$. As such, $a(t)$ is a value between -1 and 1 , where 1 indicates perfect alignment.

To compute the total alignment of a polycube segmentation $\mathcal{S}(\mathcal{M}')$, we simply use an area-weighted sum:

$$f_a(\mathcal{S}(\mathcal{M}')) = \frac{1}{\text{area}(\mathcal{M}')} \sum_{t \in \mathcal{M}'} f_a(t) * \text{area}(t)$$

Observe that the alignment score is always between -1 and 1 .

Since we have two optimization criteria, we essentially obtain a multi-objective optimization problem. To solve this problem, we use linear scalarization to turn this problem into a single-objective optimization problem. Specifically, we define the quality of a solution as

$$f(\mathcal{L}, \mathcal{S}(\mathcal{M}')) = f_a(\mathcal{S}(\mathcal{M}')) - \beta f_c(\mathcal{L}),$$

where β is a parameter that controls the trade-off between complexity and alignment. This optimization function can be interpreted as follows. For every additional loop in the loop structure, the total alignment score should increase by at least β . The parameter β can then also be used to control the complexity of the resulting polycube segmentation.

Evolutionary algorithm. To optimize the polycube loop structure, we use an evolutionary algorithm with only mutation and selection (no crossover). Specifically, our algorithm maintains a population of N loop structures, which are all initialized as described above. In each generation we generate N' offspring as follows. First, we pick a loop structure \mathcal{L} from our population uniformly at random. Then we randomly apply one of two possible mutations, each with a 50% chance. In the first mutation we randomly choose a loop ℓ to be removed from \mathcal{L} , that is, $\mathcal{L}' = \mathcal{L} \setminus \{\ell\}$. Here we restrict ourselves to loops ℓ such that \mathcal{L}' is a valid polycube loop structure (see [SSV25]

for how to compute this efficiently). For the second mutation, we choose values $3n_x$, n_y , and n_z , each uniformly at random in the range $[0, 2]$. We then add n_x X -loops, n_y Y -loops, and n_z Z -loops to \mathcal{L} as described in Section 4.1, each starting from a randomly selected position/loop region. Note that all offspring loop structures are valid polycube loop structures by construction.

Given the parent solutions and the offspring solutions, we choose a new generation by selecting the $\lceil N/2 \rceil$ best offspring solutions and the $\lfloor N/2 \rfloor$ best parent solutions. We continue this process until the best solution in a generation has not improved over the last 10 generations, at which point we return this best solution, consisting of a loop structure and a corresponding polycube segmentation, as the output of our algorithm.

5. Results

We implemented the algorithm described in Section 4, which we refer to as the DualLoops algorithm, and evaluated its performance on a diverse set of input meshes. Our evaluation primarily focuses on two key aspects: (1) the direct quality by evaluating resulting polycube segmentations and (2) the indirect quality by evaluating hexahedral meshes generated using the polycube segmentations within a polycube-based hex-meshing pipeline.

Our dataset consists of a diverse set of 3D models collected from online sources, categorized by both geometric style and topological complexity. Geometrically, we distinguish between smooth and CAD models. Smooth models typically represent organic shapes, such as animals or humans, and are widely used in computer graphics applications like animation and game development. In contrast, CAD models depict mechanical components characterized by sharp edges and flat surfaces, commonly found in engineering contexts such as aerospace or automotive design. We also separate models based on genus, as our method currently requires manual initialization for inputs with genus $g > 0$. To ensure a fair evaluation, results for higher-genus inputs are reported separately.

1. **Smooth** ($g = 0, n = 22$): airplane1, airplane2, amogus, armadillo, bimba, blub, bone, bumpysphere, bunny, buste, cat, chineselion, dino2, ghost, goathead, homer, igea, koala, moai, sphinx, spot, venus
2. **Smooth** ($g > 0, n = 6$): bottle1, bottle2, bumpytorus, cup1, dtorus, teapot
3. **CAD** ($g = 0, n = 42$): B0, B11, B12, B14, B15, B16, B17, B18, B19, B2, B20, B21, B23, B25, B27, B28, B30, B34, B35, B36, B38, B39, B40, B41, B43, B46, B48, B49, B5, B50, B57, B59, B60, B61, B68, B7, B70, B71, B75, B8, B9, fandisk
4. **CAD** ($g > 0, n = 14$): B1, B3, B10, B13, B32, B33, B51, B62, B65, B66, B73, block, rocker, rod

We compare DualLoops with two publicly available polycube segmentation algorithms: PolyCut [LVS*13] and EvoCube [DPM*22]. For PolyCut, EvoCube, and RobustPolycube we used default parameters; for our method we used $N = 10$, $N' = 30$, $\alpha = 10$, and $\beta = 0.01$.

	$f_a(\mathcal{M})$	$f'_c(\mathcal{M})$
PolyCut	0,911	29
Smooth ($g = 0$)	0,843	38
Smooth ($g > 0$)	0,840	67
CAD ($g = 0$)	0,943	22
CAD ($g > 0$)	0,943	27
EvoCube	0,886	99
Smooth ($g = 0$)	0,797	296
Smooth ($g > 0$)	0,847	68
CAD ($g = 0$)	0,915	20
CAD ($g > 0$)	0,943	29
DualLoops	0,906	29
Smooth ($g = 0$)	0,836	38
Smooth ($g > 0$)	0,848	55
CAD ($g = 0$)	0,941	20
CAD ($g > 0$)	0,942	27

Table 1: Comparison of polycube segmentations from PolyCut [LVS*13], EvoCube [DPM*22], and our method (DualLoops).

5.1. Polycube segmentation quality

We briefly compare the resulting polycube segmentations generated by the three methods (PolyCut, EvoCube, and our DualLoops) by using the alignment criteria computed using $f_a(\mathcal{M})$ mentioned in Section 4. The complexity criteria (the number of loops) cannot be computed easily for the outer methods, as such, we opt for the following: we compute the the irregular polycube corners in the segmentation (the number of vertices with more than 2 different labels adjacent to it) and list the values in the column $f'_c(\mathcal{M})$. Note that we cannot compute any validity criteria on the resulting polycube segmentations. The resulting polycube segmentations from our methods are guaranteed to be valid. The polycube segmentations resulting from the other methods may not be valid.

5.2. Hexahedral meshing

To ensure a fair comparison, we evaluate the algorithms within a unified polycube-based hexahedral meshing pipeline. Specifically, we use the polycube segmentations generated by all three methods (PolyCut, EvoCube, and our DualLoops) as input for RobustPolycube [PRR*22] to compute hexahedral meshes. As a result, the results for PolyCut and EvoCube may differ from those reported in prior work, where different downstream pipelines or parameter settings may be used.

The evaluation of the hexahedral meshes involves computing cell quality via the scaled Jacobian [PCS*22], vertex quality via vertex irregularity [PCS*22], and geometric fidelity using the Hausdorff distance [GLYL20, FXBH16, HJS*14]. It is important to note that EvoCube is a randomized algorithm, as is our own. Therefore, different runs may yield different results. We report on the number of failed cases, instances where the hexahedral mesher cannot process

the given segmentation (typically due to an invalid polycube segmentation). These failures are not penalized in the average quality metrics; instead, all evaluations are computed over the subset of successful outputs. For reproducibility, we briefly explain how these metrics are computed.

The Scaled Jacobian (SJ) of a hexahedral cell h that is part of a hexahedral mesh \mathcal{H} is the minimum of the Jacobian determinants at each vertex of h , normalized by the lengths of the three adjacent edges (e_1 , e_2 , and e_3):

$$\text{SJ}(h) = \min_{v \in h} \left(\frac{\det J(v)}{|e_1| \cdot |e_2| \cdot |e_3|} \right)$$

We report on the minimum and average SJ across all cells in \mathcal{H} . Hexahedral meshes with cells with $\text{SJ}(h) < 0$ (inverted or degenerate cells) are typically unusable for simulation.

We measure mesh irregularity (%irr) via the percentage of irregular vertices. A vertex of a hexahedral mesh is *regular* if it is adjacent to 2, 4, or 8 hexahedral cells, and *irregular* otherwise. Similarity between the input model \mathcal{M} and the surface of hexahedral mesh \mathcal{H} is measured using the symmetric Hausdorff distance $\overline{\text{HD}}$. We normalize the Hausdorff distance by dividing it by the length of the diagonal of the axis-aligned bounding box encompassing \mathcal{M} (the scale of \mathcal{M}). We further multiply the Hausdorff distance by 100 to facilitate a concise presentation of the results.

The hexahedral meshes are visualized using HexaLab [BTP*19], with the hex quality color setting showing the Scaled Jacobian of the cells.

5.3. Discussion

Quantitative results can be found in Table 1 (quality of polycube segmentations) and Table 2 (quality of resulting hexahedral meshes). The resulting polycube segmentations from PolyCut and our method (DualLoops) are of mostly similar quality. The polycube segmentations by EvoCube have a slightly lower alignment, and a higher complexity. Recall that our method is guaranteed to always return a valid polycube segmentation. This results in the hex-meshing pipeline to always succeed when given our polycube segmentations. The hex-meshing pipeline failed for some results of PolyCut (7) and EvoCube (3). Furthermore, the hexahedral meshes resulting from our polycube segmentations often are of higher quality than those constructed via the other methods in terms of the Scaled Jacobian, irregularity, and similarity (measured through the Hausdorff distance).

Qualitative results can be seen in Figure 8 (comparison of polycube segmentations and resulting hexahedral meshes) and Figure 9 (showcase of dual loops, polycube segmentations and polycubes). For models that contain features well-aligned with the principal axes, all three methods result in similar polycube segmentations, and as a result, similar hexahedral meshes. On the contrary, our algorithm sometimes fails to capture features well that are not aligned with any of the principal directions, such as the horns of *goat-head*. Small features, such as the hands and toes of *armdillo* and *homeer*, require multiple specific loops to be captured well.

	[!]	SJ _{min}	SJ _{avg}	%irr	$\overline{\text{HD}}$
PolyCut	7	0,042	0,913	0,032	2,212
Smooth ($g = 0$)	1	-0,041	0,911	0,026	2,009
Smooth ($g > 0$)	4	0,017	0,883	0,027	1,249
CAD ($g = 0$)	2	0,063	0,908	0,036	2,421
CAD ($g > 0$)	0	0,112	0,937	0,030	2,058
EvoCube	3	0,025	0,908	0,035	2,534
Smooth ($g = 0$)	0	-0,081	0,909	0,036	3,037
Smooth ($g > 0$)	1	0,046	0,904	0,023	1,450
CAD ($g = 0$)	2	0,048	0,899	0,038	2,511
CAD ($g > 0$)	0	0,117	0,933	0,030	2,197
DualLoops	0	0,076	0,919	0,031	2,200
Smooth ($g = 0$)	0	0,059	0,911	0,030	1,921
Smooth ($g > 0$)	0	0,079	0,913	0,019	1,485
CAD ($g = 0$)	0	0,073	0,917	0,034	2,522
CAD ($g > 0$)	0	0,111	0,941	0,027	1,977

Table 2: Comparison of hexahedral meshes constructed from polycube segmentations from PolyCut [LVS*13], EvoCube [DPM*22], and our method (DualLoops), via the polycube-based hexahedral mesh pipeline RobustPolycube [PRR*22].

6. Conclusion

We presented an iterative algorithm for constructing polycube segmentations of 3D models, guaranteed to produce valid solutions, even for inputs with higher genus. Our method leverages a recent dual characterization of polycubes [SSV25] to initialize a simple, valid polycube of the appropriate genus and iteratively refine it alongside its dual loop structure. Throughout the refinement process, the validity of the solution is maintained. Our experiments demonstrate that the final polycube segmentations match or exceed the quality of state-of-the-art approaches.

A key limitation of our method is the need for a *manual* initialization step on high-genus inputs. While we believe that an automated initialization procedure is feasible, we do not yet have a robust solution for it.

Furthermore, our work focuses solely on generating the polycube segmentation. The downstream applications may require the accompanying polycube with additional constraints, such as non-intersecting geometry, integer vertex coordinates, or fixed edge lengths. Fortunately, the dual structure naturally lends itself to polycube construction. As such, addressing these constraints and incorporating the resulting mapping distortion into our framework are natural directions for future work.

Finally, our current loop computations rely on alignment with the principal axes. While this often produces high-quality results, certain inputs may benefit from loops that slightly deviate from axis alignment. A natural extension of our method is to incorporate more expressive direction fields into the loop computation process.

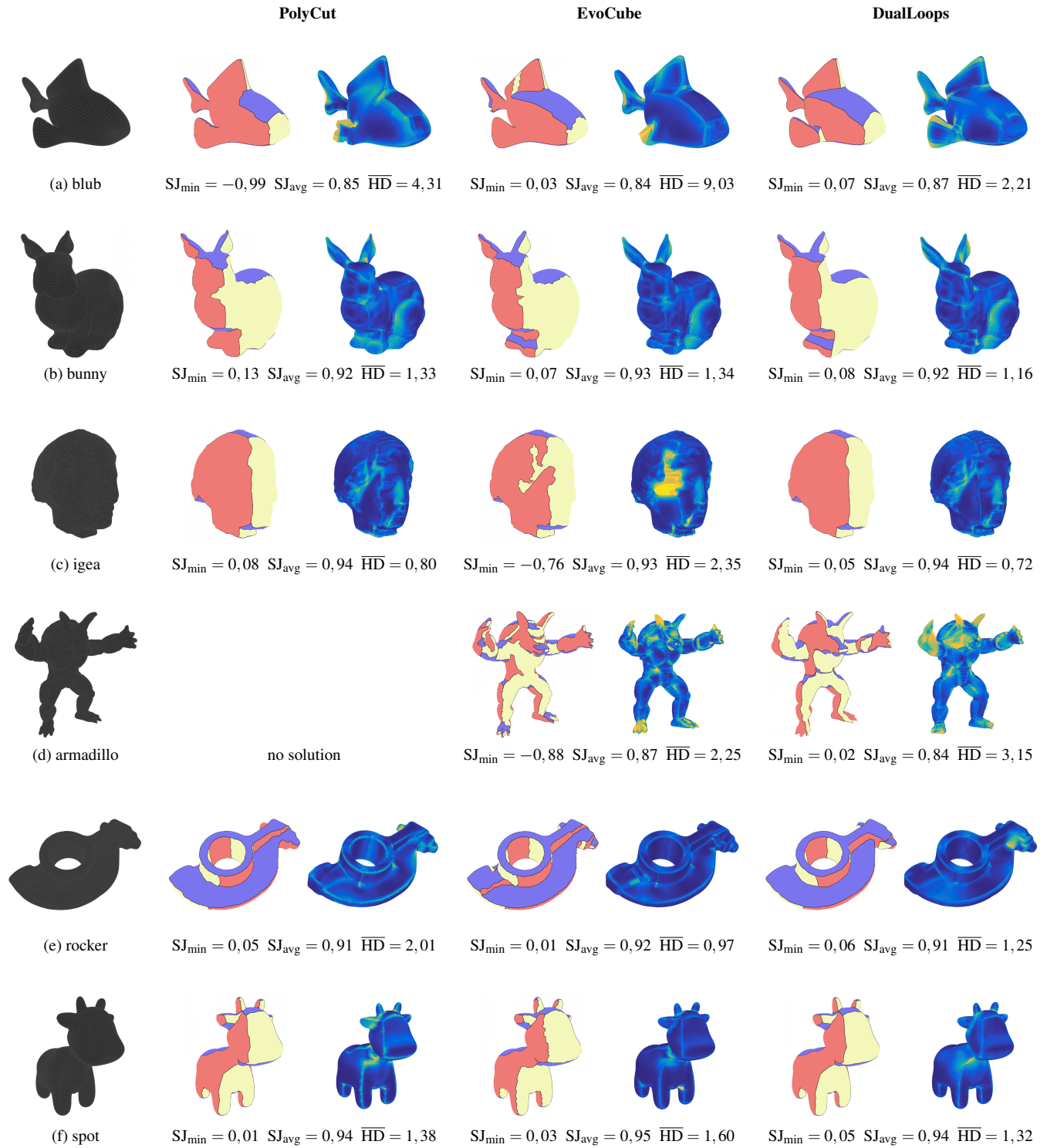


Figure 8: Comparison of the three methods PolyCut [LVS*13], EvoCube [DPM*22], and our method DualLoops. We show the input mesh, and polycube segmentation and resulting hexahedral meshes per method. We include the values for SJ_{\min} , SJ_{avg} , and \overline{HD} per hexahedral mesh.

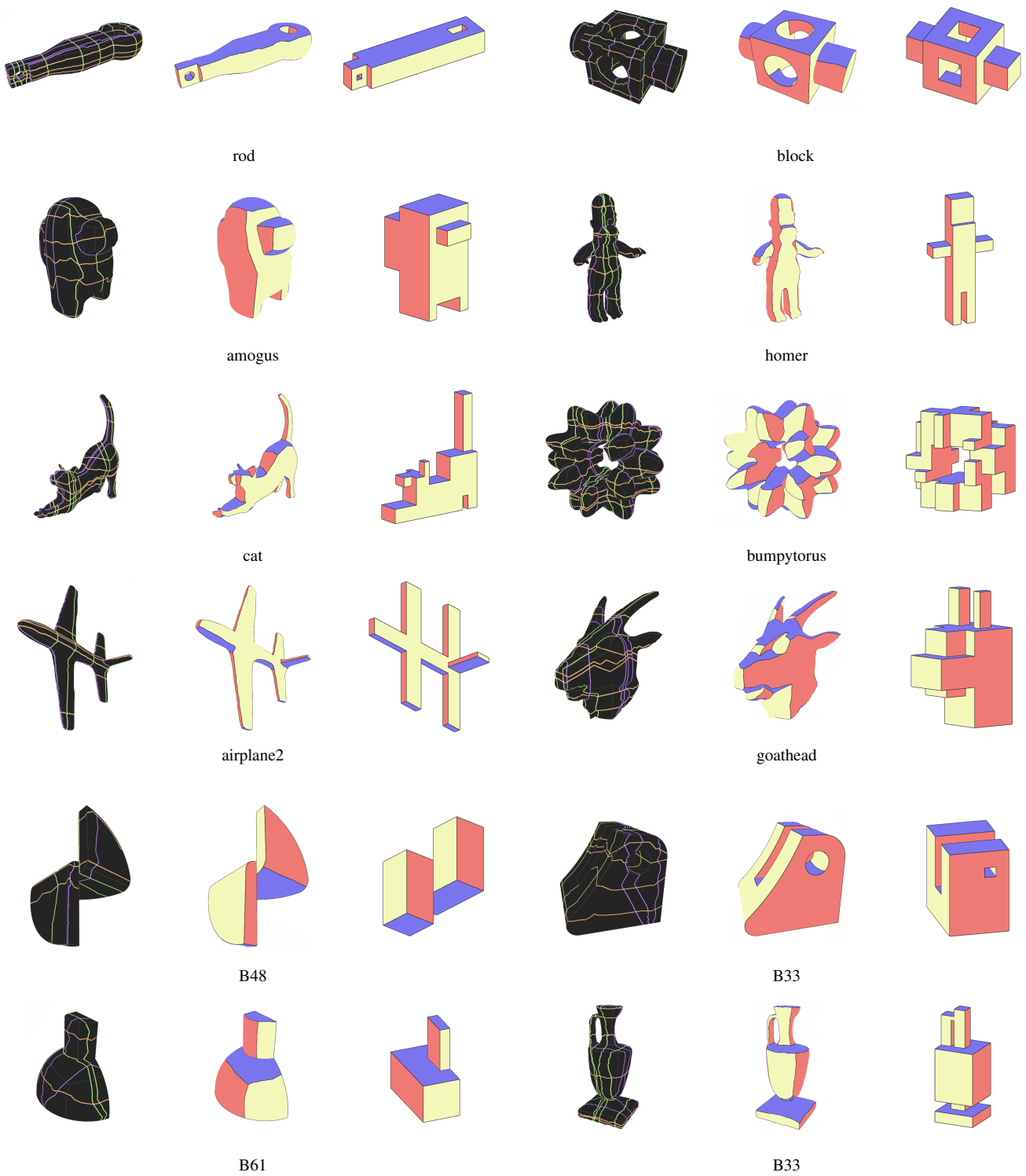


Figure 9: Showcase of results generated by our DualLoops algorithm, illustrating the transformation from loop structure to polycube segmentation and corresponding polycube.

References

- [BBG*09] BOELENS O., BADCOCK K., GÖRTZ S., MORTON S., FRITZ W., KARMAN S., MICHAL T., LAMAR J.: F-16xl geometry and computational grids used in cranked-arrow wing aerodynamics project international. *Journal of Aircraft* 46 (2009). doi:10.2514/1.34852. 1
- [BG04] BIEDL T., GENC B.: When can a graph form an orthogonal polyhedron? In *Proceedings of the 16th Canadian Conference on Computational Geometry (CCCG)* (2004). URL: www.cccg.ca/proceedings/2004/15.pdf. 2, 3
- [BK23] BAUMEISTER M., KOBBELT L.: How close is a quad mesh to a polycube? *Computational Geometry* 111 (2023). doi:10.1016/j.comgeo.2022.101978. 2
- [BTP*19] BRACCI M., TARINI M., PIETRONI N., LIVESU M., CIGNONI P.: Hexalab.net: An online viewer for hexahedral meshes. *Computer-Aided Design* 110 (2019). doi:10.1016/j.cad.2018.12.003. 9
- [CBK12] CAMPEN M., BOMMES D., KOBBELT L.: Dual loops meshing: quality quad layouts on manifolds. *ACM Transactions on Graphics* 31, 4 (2012). doi:10.1145/2185520.2185606. 2
- [CLS16] CHERCHI G., LIVESU M., SCATENI R.: Polycube simplification for coarse layouts of surfaces and volumes. *Computer Graphics Forum* 35, 5 (2016). doi:10.1111/cgf.12959. 2
- [DPM*22] DUMERY C., PROTAIS F., MESTRALLET S., BOURCIER C., LEDOUX F.: Evocube: A genetic labelling framework for polycube-maps. *Computer Graphics Forum* 41, 6 (2022). doi:10.1111/cgf.14649. 1, 2, 8, 9, 10
- [EM10] EPPSTEIN D., MUMFORD E.: Steinitz theorems for orthogonal polyhedra. In *Proceedings of the 26th Annual Symposium on Computational Geometry (SoCG)* (2010). doi:10.1145/1810959.1811030. 2
- [FBL16] FU X.-M., BAI C.-Y., LIU Y.: Efficient volumetric polycube-map construction. *Computer Graphics Forum* 35, 7 (2016). doi:10.1111/cgf.13007. 2
- [FXBH16] FANG X., XU W., BAO H., HUANG J.: All-hex meshing using closed-form induced polycube. *ACM Transactions on Graphics* 35, 4 (2016). doi:10.1145/2897824.2925957. 2, 8
- [GLYL20] GUO H.-X., LIU X., YAN D.-M., LIU Y.: Cut-enhanced polycube-maps for feature-aware all-hex meshing. *ACM Transactions on Graphics* 39, 4 (2020). doi:10.1145/3386569.3392378. 2, 8
- [GSZ11] GREGSON J., SHEFFER A., ZHANG E.: All-hex mesh generation via volumetric polycube deformation. *Computer Graphics Forum* 30, 5 (2011). doi:10.1111/j.1467-8659.2011.02015.x. 1, 2
- [HJS*14] HUANG J., JIANG T., SHI Z., TONG Y., BAO H., DESBRUN M.: 11-based construction of polycube maps from complex shapes. *ACM Transactions on Graphics* 33, 3 (2014). doi:10.1145/2602141. 2, 8
- [HLW*24] HE L., LEI N., WANG Z., WANG C., ZHENG X., LUO Z.: Expanding the solvable space of polycube-map via validity-enhanced construction. In *Proceedings of the 2024 SIAM International Meshing Roundtable (IMR)* (2024). doi:10.1137/1.9781611978001.4. 2
- [HWFQ09] HE Y., WANG H., FU C.-W., QIN H.: A divide-and-conquer approach for automatic polycube map construction. *Computers & Graphics* 33, 3 (2009). doi:10.1016/j.cag.2009.03.024. 2
- [HZ16] HU K., ZHANG Y. J.: Centroidal voronoi tessellation based polycube construction for adaptive all-hexahedral mesh generation. *Computer Methods in Applied Mechanics and Engineering* 305 (2016). doi:10.1016/j.cma.2016.03.021. 2
- [HZL17] HU K., ZHANG Y. J., LIAO T.: Surface segmentation for polycube construction based on generalized centroidal voronoi tessellation. *Computer Methods in Applied Mechanics and Engineering* 316 (2017). doi:10.1016/j.cma.2016.07.005. 2
- [LJFW08] LIN J., JIN X., FAN Z., WANG C. C. L.: Automatic polycube-maps. In *Advances in Geometric Modeling and Processing (GMP)* (2008). doi:10.1007/978-3-540-79246-8_1. 2
- [LVS*13] LIVESU M., VINING N., SHEFFER A., GREGSON J., SCATENI R.: Polycut: monotone graph-cuts for polycube base-complex construction. *ACM Transactions on Graphics* 32, 6 (2013). doi:10.1145/2508363.2508388. 1, 2, 8, 9, 10
- [MCBC22] MANDAD M., CHEN R., BOMMES D., CAMPEN M.: Intrinsic mixed-integer polycubes for hexahedral meshing. *Computer Aided Geometric Design* 94 (2022). doi:10.1016/j.cagd.2022.102078. 2
- [MPBL23] MESTRALLET S., PROTAIS F., BOURCIER C., LEDOUX F.: Limits and prospects of polycube labelings. In *Research notes of the 2023 SIAM International Meshing Roundtable (IMR)* (2023). URL: cea.hal.science/cea-04169841/. 2
- [PCS*22] PIETRONI N., CAMPEN M., SHEFFER A., CHERCHI G., BOMMES D., GAO X., SCATENI R., LEDOUX F., REMACLE J., LIVESU M.: Hex-mesh generation and processing: A survey. *ACM Transactions on Graphics* 42, 2 (2022). doi:10.1145/3554920. 1, 2, 8
- [PRR*22] PROTAIS F., REBEROL M., RAY N., CORMAN E., LEDOUX F., SOKOLOV D.: Robust quantization for polycube maps. *Computer-Aided Design* 150 (2022). doi:10.1016/j.cad.2022.103321. 2, 8, 9
- [Sok16] SOKOLOV D.: *Modélisation géométrique*. Habilitation à diriger des recherches, Université de Lorraine, 2016. URL: inria.hal.science/tel-03180395/. 2
- [SR15] SOKOLOV D., RAY N.: *Fixing normal constraints for generation of polycubes*. research report, LORIA, 2015. URL: inria.hal.science/hal-01211408/. 2
- [SSV25] SNOEP M., SPECKMANN B., VERBEEK K.: Polycubes via dual loops. In *Proceedings of the 2025 SIAM International Meshing Roundtable (IMR)* (2025). To appear. URL: www.arxiv.org/abs/2410.16865. 2, 3, 5, 7, 9
- [THCM04] TARINI M., HORMANN K., CIGNONI P., MONTANI C.: Polycube-maps. *ACM Transactions on Graphics* 23, 3 (2004). doi:10.1145/1015706.1015810. 1, 2
- [WHL*07] WANG H., HE Y., LI X., GU X., QIN H.: Polycube splines. In *Proceedings of the 2007 ACM Symposium on Solid and Physical Modeling (SPM)* (2007). doi:10.1145/1236246.1236281. 1
- [WHL*08] WANG H., HE Y., LI X., GU X., QIN H.: Polycube splines. *Computer-Aided Design* 40, 6 (2008). doi:10.1016/j.cad.2008.01.012. 2
- [WYZ*11] WAN S., YIN Z., ZHANG K., ZHANG H., LI X.: A topology-preserving optimization algorithm for polycube mapping. *Computers & Graphics* 35, 3 (2011). doi:10.1016/j.cag.2011.03.018. 2
- [YFL19] YANG Y., FU X.-M., LIU L.: Computing surface polycube-maps by constrained voxelization. *Computer Graphics Forum* 38, 7 (2019). doi:10.1111/cgf.13838. 2
- [YZWL14] YU W., ZHANG K., WAN S., LI X.: Optimizing polycube domain construction for hexahedral remeshing. *Computer-Aided Design* 46 (2014). doi:10.1016/j.cad.2013.08.018. 2
- [ZLL*17] ZHAO H., LEI N., LI X., ZENG P., XU K., GU X.: Robust edge-preserved surface mesh polycube deformation. In *Proceedings of the 25th Pacific Conference on Computer Graphics and Applications (PG)* (2017). doi:10.2312/pg.20171319. 2
- [ZLW*19] ZHAO H., LI X., WANG W., WANG X., WANG S., LEI N., GU X.: Polycube shape space. *Computer Graphics Forum* 38, 7 (2019). doi:10.1111/cgf.13839. 2